34th Annual International Conference of the IEEE EMBS
San Diego, California USA, 28 August - 1 September, 2012

Study of Magnetization Evolution by Using Composite Spin-lock Pulses for $T_{1\rho}$ Imaging

Yujia LI, Feng ZHAO, Yi-Xiang WANG, Anil T AHUJA, Jing YUAN

***Abstract*— B_0 and B_1 field inhomogeneities may generate banding-like artifacts in $T_1\rho$-weighted images and hence result in errors of $T_{1\rho}$ quantification. Several types of composite spin-lock pulses have been proposed to alleviate such artifacts. In this study, magnetization evolution with $T_{1\rho}$ and $T_{2\rho}$ relaxation by using these composite spin-lock pulses are theoretically derived. The effectiveness and limitation of each spin-lock pulse are explicitly illustrated in mathematical forms and phantom $T_{1\rho}$-weighted images acquired by using each spin-lock pulse are presented. This study also provides a theoretical framework for $T_{1\rho}$ quantification from $T_{1\rho}$-weighted images even with B_0 and B_1 inhomogeneity artifacts.**

I. Introduction

$T_{1\rho}$ is the time constant of the transverse magnetization decay given the application of a spin-lock pulse, which is aligned with the net magnetization vector. $T_{1\rho}$ relaxation is able to create tissue contrast different from the conventional MRI contrasts based on T_1 and T_2 relaxation. $T_{1\rho}$ relaxation contrast is sensitive to low frequency motional processes, and is potential for many clinical applications [1-6].

Conventionally, a three-pulse cluster including tip-down, spin-lock and tip-up pulse is used to generate $T_{1\rho}$-weighted images. However, in the presence of inhomogeneous B_0 and B_1 field, the net magnetization may not align with the spin-lock field any longer, and accordingly result in a complicated magnetization evolution and hence banding-like artifact on $T_{1\rho}$-weighted images. Composite spin-lock pulses have been proposed to reduce the artifacts. In this paper, we present a review of several types of composite spin-lock pulses and the magnetization evolutions with $T_{1\rho}$ and $T_{2\rho}$ relaxation by using each spin-lock pulse are theoretically derived. The relationship between the magnetization and various factors of spin-lock time, spin-lock frequencies, B_0 and B_1 inhomogeneities are illustrated.

II. Theory

A. Conventional spin-lock pulse: 90_x-TSL_y-90_{-x}

A conventional spin-lock pulse (Fig. 1) consists of three pulses: an initial hard pulse along x direction to tip-down the net magnetization to the transverse plane, a hard spin-lock pulse with duration of TSL to excite $T_{1\rho}$ relaxation, and a final hard pulse along –x direction to tip-up the net magnetization from the transverse plane to the longitudinal plane. Principally, the magnetization aligned with the spin-lock field decays with $T_{1\rho}$ and the magnetization perpendicular to the spin-lock field decays with $T_{2\rho}$.

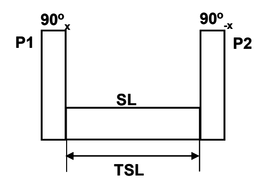

Figure 1. The schematic of conventional spin-lock pulse.

The magnetization evolution during the application of a pulse can be traced by using the Block Equation. For description, an RF pulse is represented in the form of matrix notation $R_\varphi(\Phi)$, where R denotes a rotation matrix, φ is the pulse orientation and Φ is the pulse flip angle. β is the flip angle of tip-down/tip-up pulse and ∂ is the flip angle of each SL segment. Given spin-lock frequency FSL, $\partial=2\pi\cdot FSL\cdot TSL$. E_ρ is a matrix to describe $T_{1\rho}$ and $T_{2\rho}$ relaxation. The basic rotation matrices that rotate spin vectors about the x, y, or z axis by an angle Φ in three dimensions, and E_ρ are expressed as in Equation (1),

$$R_x(\Phi)=\begin{bmatrix}1 & 0 & 0\\ 0 & \cos\Phi & \sin\Phi\\ 0 & -\sin\Phi & \cos\Phi\end{bmatrix};\ R_y(\Phi)=\begin{bmatrix}\cos\Phi & 0 & -\sin\Phi\\ 0 & 1 & 0\\ \sin\Phi & 0 & \cos\Phi\end{bmatrix};$$

$$R_z(\Phi)=\begin{bmatrix}\cos\Phi & \sin\Phi & 0\\ -\sin\Phi & \cos\Phi & 0\\ 0 & 0 & 1\end{bmatrix};\ E_\rho=\begin{bmatrix}e^{-TSL/2T_{2\rho}} & 0 & 0\\ 0 & e^{-TSL/2T_{2\rho}} & 0\\ 0 & 0 & e^{-TSL/2T_{1\rho}}\end{bmatrix} \quad (1)$$

The relaxation during P1 and P2 is usually negligible due to their much shorter pulse duration than the TSL. The magnetization evolution is expressed as in Equation (2),

$$M(t)=R_{-x}(\beta)\cdot R_y(\partial)E_\rho\cdot R_x(\beta)\cdot M(t_0)$$
$$\Rightarrow M_z=M_0\cdot(\sin^2\beta\cdot e^{-TSL/T_1\rho}+\cos^2\beta\cos\partial\cdot e^{-TSL/T_{2\rho}}) \quad (2)$$

Where $M(t_0)=[0\ 0\ M_0]'$. When the tip-down/tip-up pulse has a perfect flip angle of 90°, the resulting longitudinal magnetization is simply related to $T_{1\rho}$ relaxation as the normal mono-exponential relaxation model shown in Equation (3),

$$M_z=M_0\cdot e^{-TSL/T_1\rho} \quad (3)$$

Given imperfect tip-down/tip-up flip angles, a magnetization precession around the spin-lock field occurs (Fig. 2). A flip angle of ∂ is formed as the magnetization precesses from point 1 to point 2 during TSL. As a result, this pulse is B_1 sensitive as ∂ is related to B_1.

* This work is supported by HK ITF grant ITS/021/10 and RGC grant SEG_CUHK02.

Yujia LI (yjli@cuhk.edu.hk), Feng ZHAO (zhaofeng@cuhk.edu.hk), Yi-Xiang WANG (yixiang_wang@cuhk.edu.hk), Anil T AHUJA (aniltahuja@cuhk.edu.hk) and Jing YUAN (corresponding author, phone: 852-2632-1036; jyuanbwh@gmail.com) are with Department of Imaging and Interventional Radiology, The Chinese University of Hong Kong, Shatin, N.T., Hong Kong.

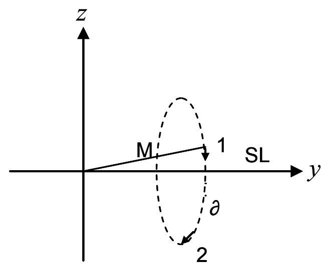

Figure 2. Magnetization precession of conventional spin-lock pulse.

B. Rotary-echo spin-lock pulse: 90_x-$TSL/2_y$- $TSL/2_{-y}$ -90_{-x}

This pulse divides a spin-lock pulse into two segments which have opposite phase shifts (Fig. 3) and tends to remove the artifact resulted from the flip angle of SL pulse ∂ [7]. During SL1, the magnetization M precesses from point 1 to point 2 with flip angle of ∂ and then precesses from point 2 to point 3 during SL2 (Fig. 4). Given the same duration of SL1 and SL2, point 3 is identical as point 1. The resulting longitudinal magnetization will be irrelevant with ∂. The magnetization evolution is expressed as in Equation (4),

$$M(t) = R_{-x}(\beta)\cdot R_{-y}(\partial)E_\rho \cdot R_y(\partial)E_\rho \cdot R_x(\beta)\cdot M(t_0)$$
$$\Rightarrow M_z = M_0 \cdot (\sin^2\beta \cdot e^{-TSL/T_{1\rho}} + \cos^2\beta \cdot e^{-TSL/T_{2\rho}}) \quad (4)$$

When tip-down/tip-up flip angle equals to 90^o, the resulting longitudinal magnetization is simplified as Equation (3). Note that image could still be contaminated by $T_{2\rho}$ contrast in the presence of B_1 field inhomogeneity according to Equation (4) when $\beta \neq 90^o$.

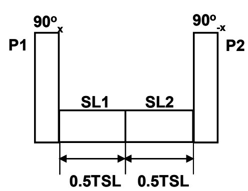

Figure 3. The schematic of rotary-echo spin-lock pulse.

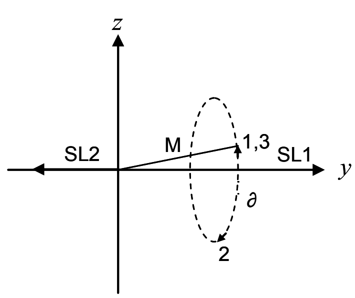

Figure 4. Magnetization precession of rotary-echo spin-lock pulse.

Equation (4) is derived with the assumption of homogeneous B_0. When there is an offset of ΔB_0, the effective spin-lock field will change to z' and z'' given the application of SL1 and SL2 respectively (Fig. 5), where $\theta = \tan^{-1}(\omega_1/\Delta\omega) = \tan^{-1}(B_1/\Delta B_0)$ is the angle from the effective spin-lock field to z-axis. M precesses initially from point 1 to point 2 during SL1 and then precesses from point 2 to point 3 during SL2. The magnetization evolution becomes much more complicated as shown in Equation (5).

$$M(t) = R_{-x}(\beta)\cdot R_{z''}(\partial)E_\rho \cdot R_{z'}(\partial)E_\rho \cdot R_x(\beta)\cdot M(t_0)$$
$$= R_{-x}(\beta)\cdot R_x(-\theta)R_z(\partial)E_\rho R_x(\theta)\cdot R_x(\theta)R_z(\partial)E_\rho R_x(-\theta)\cdot R_x(\beta)\cdot M(t_0)$$
$$\Rightarrow M_z = M_0 \cdot [\cos 2\theta(\cos^2\beta - \sin^2\theta)\cdot e^{-TSL/T_{1\rho}}$$
$$+ (\cos^2\beta - \cos^2\theta)(\sin^2\partial - \cos^2\partial\cos 2\theta)\cdot e^{-TSL/T_{2\rho}}$$
$$+ \cos\partial \sin^2 2\theta \cdot e^{-0.5\cdot TSL/T_{1\rho}} \cdot e^{-0.5\cdot TSL/T_{2\rho}}] \quad (5)$$

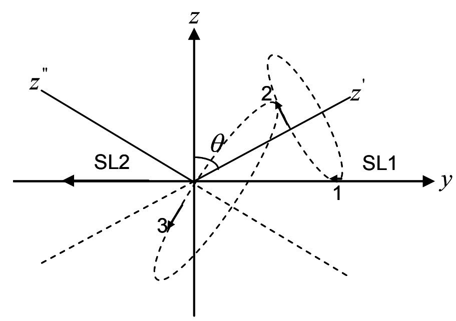

Figure 5. Magnetization precession of rotary-echo spin-lock pulse in inhomogeneous B_0 field.

If $\omega_1 >> \Delta\omega$, $\theta = 90^o$, Equation (5) is identical as Equation (4). If $\omega_1 << \Delta\omega$, $\theta = 0^o$, Equation (5) is simplified as shown in Equation (6),

$$M_z = M_0 \cdot [\cos^2\beta \cdot e^{-TSL/T_{1\rho}} + \sin^2\beta\cos(2\partial)\cdot e^{-TSL/T_{2\rho}}] \quad (6)$$

When $\beta = 90^o$, trace of $T_{1\rho}$ relaxation will be lost and only $T_{2\rho}$ relaxation can be traced by Equation (6).

If $\omega_1 \sim \Delta\omega$ and $\beta = 90^o$, Equation (5) is simplified as shown in Equation (7) and artifacts will be serious [8],

$$M_z = M_0 \cdot [-\cos 2\theta \sin^2\theta \cdot e^{-TSL/T_{1\rho}}$$
$$- \cos^2\theta(\sin^2\partial - \cos^2\partial\cos 2\theta)\cdot e^{-TSL/T_{2\rho}}$$
$$+ \cos\partial \sin^2 2\theta \cdot e^{-0.5\cdot TSL/T_{1\rho}} \cdot e^{-0.5\cdot TSL/T_{2\rho}}] \quad (7)$$

C. B_1 and B_0 insensitive composite spin-lock pulse: 90_x-$TSL/2_y$- 180_y- $TSL/2_{-y}$ -90_{-x}

This spin-lock pulse inserts a refocusing pulse between rotary-echo spin-lock pulse segments (Fig. 6) so as to cancel the flip angle of spin-lock pulse in imperfect B_0 field [9]. During SL1, M precesses from point 1 to point 2 and then is reversed by the refocusing pulse, precessing 180^o around y-axis to point 3. During SL2, M precesses from point 3 to point 4 which is identical as point 1. Hence, the resulting magnetization is irrelevant with ∂. The magnetization evolution is expressed as in Equation (8),

$$\begin{aligned}
M(t) &= R_{-x}(\beta)\cdot R_{z'}(\partial)E_\rho \cdot R_y(2\beta)\cdot R_{z'}(\partial)E_\rho \cdot R_x(\beta)\cdot M(t_0)\\
&= R_{-x}(\beta)\cdot R_x(-\theta)R_z(\partial)E_\rho R_x(\theta)\cdot R_y(2\beta)\cdot R_x(\theta)R_z(\partial)E_\rho R_x(-\theta)\cdot R_x(\beta)\cdot M(t_0)\\
\Rightarrow M_z &= M_0\cdot[e^{-TSL/T_{1\rho}}\cdot(\cos^2\beta-\sin^2\theta)(\cos^2\theta\cos2\beta-\sin^2\theta)\\
&\quad + e^{-TSL/T_{2\rho}}\cdot(\cos^2\beta-\cos^2\theta)\\
&\quad \cdot(-\cos^2\partial\cos^2\theta+\cos(2\beta)\sin^2\partial+\cos(2\beta)\cos^2\partial\sin^2\theta)\\
&\quad + \frac{1}{2}e^{-0.5\cdot TSL/T_{1\rho}}e^{-0.5\cdot TSL/T_{2\rho}}\cdot(1+\cos(2\beta))\\
&\quad \cdot(\cos\partial\sin^2(2\theta)+2\sin\partial\cos\theta-2\cos(2\beta)\sin\partial\cos\theta)]
\end{aligned} \tag{8}$$

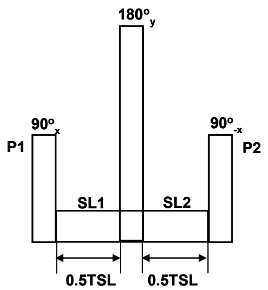

Figure 6. The schematic of B_1 and B_0 insensitive composite spin-lock pulse.

If β=90°, Equation (8) is simplified as Equation (9),

$$M_z = M_0(\sin^2\theta\cdot e^{-TSL/T_{1\rho}} + \cos^2\theta\cdot e^{-TSL/T_{2\rho}}) \tag{9}$$

The resulting longitudinal magnetization will be irrelevant with ∂. If $\omega_1 >> \Delta\omega$, θ=90°, Equation (9) is simplified as Equation (3). If $\omega_1 << \Delta\omega$, θ=0°, Equation (9) is simplified as Equation (10) which is a mono-exponential $T_{2\rho}$ relaxation model,

$$M_z = M_0\cdot e^{-TSL/T_{2\rho}} \tag{10}$$

If β≠90°, provided $\omega_1 >> \Delta\omega$, θ=90° and $\omega_1 << \Delta\omega$, θ=0°, Equation (10) is simplified as Equation (11) and (12) respectively and artifacts will occur.

$$M_z = M_0\cdot[e^{-TSL/T_{1\rho}}\cdot\sin^2\beta + e^{-TSL/T_{2\rho}}\cdot\cos^2\beta\cos(2\beta)] \tag{11}$$

$$\begin{aligned}
M_z &= M_0\cdot[e^{-TSL/T_{1\rho}}\cdot\cos^2\beta\cos(2\beta)\\
&\quad + e^{-TSL/T_{2\rho}}\cdot\sin^2\beta(\cos^2\partial-\sin^2\partial\cos(2\beta))\\
&\quad + e^{-0.5\cdot TSL/T_{1\rho}}e^{-0.5\cdot TSL/T_{2\rho}}\cdot\sin^2(2\beta)\sin\partial]
\end{aligned} \tag{12}$$

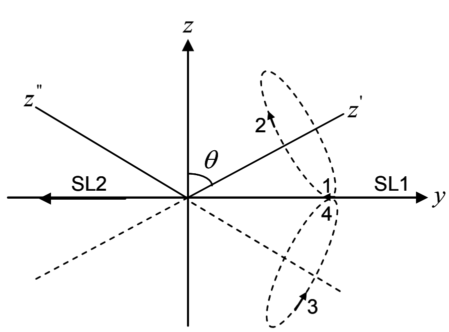

Figure 7. Magnetization precession of B_1 and B_0 insensitive composite spin-lock pulse.

D. Revised B_1 and B_0 insensitive composite spin-lock pulse: 90_x-TSL/2_y- 180_y- TSL/2_{-y} -90_x

As shown in Section II.C, B_1 and B_0 insensitive composite spin-lock pulse loses its effectiveness when β is not 90°. The revised composite spin-lock pulse is robust for imperfect tip-down/tip-up flip angle [10]. The last tip-up pulse is modified to be aligned with x-axis (Fig. 8) and tips the magnetization to –z-axis. Given imperfect tip-down/tip-up flip angle, M precesses around z' from point 1 to point 2 during SL1 and then precesses from point 2 to point 3 with the function of refocusing pulse. During SL2, M precesses from point 3 to point 4 around z''. Point 4 and point 1 should be symmetric about y-axis. Lastly, with the tip-up pulse, M will perfectly return to –z-axis. The process can remove the contaminations from imperfect tip-down/tip-up flip angle, while 180° flip angle of refocusing pulse is still necessary. Supposing δ is the flip angle of refocusing pulse, the magnetization evolution is expressed as in Equation (13),

$$\begin{aligned}
M(t) &= R_x(\beta)\cdot R_{z'}(\partial)E_\rho\cdot R_y(\delta)\cdot R_{z'}(\partial)E_\rho\cdot R_x(\beta)\cdot M(t_0)\\
&= R_x(\beta)\cdot R_x(-\theta)R_z(\partial)E_\rho R_x(\theta)\cdot R_y(\delta)\cdot R_x(\theta)R_z(\partial)E_\rho R_x(-\theta)\cdot R_x(\beta)\cdot M(t_0)\\
\Rightarrow M_z &= M_0\cdot[e^{-TSL/T_{1\rho}}\cdot\cos^2(\beta-\theta)(\cos\delta\cos^2\theta-\sin^2\theta)\\
&\quad + e^{-TSL/T_{2\rho}}\cdot\sin^2(\beta-\theta)(-\cos^2\partial\cos^2\theta+\cos\delta\sin^2\partial+\cos\delta\cos^2\partial\sin^2\theta)\\
&\quad + \frac{1}{2}e^{-0.5\cdot TSL/T_{1\rho}}e^{-0.5\cdot TSL/T_{2\rho}}\cdot(1+\cos\delta)\cos\delta\cos\partial\sin(2\theta)(\sin(2\theta)-\cos(2\theta))]
\end{aligned} \tag{13}$$

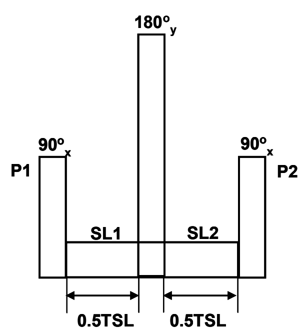

Figure 8. The schematic of revised B_1 and B_0 insensitive composite spin-lock pulse.

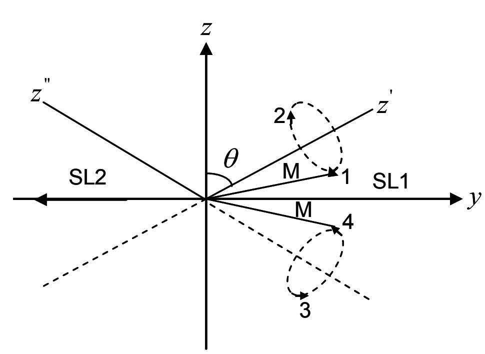

Figure 9. Magnetization precession of revised B_1 and B_0 insensitive composite spin-lock pulse.

If δ=180°, Equation (13) is simplified as Equation (14),

$$M_z = -M_0\cdot[e^{-TSL/T_{1\rho}}\cdot\cos^2(\beta-\theta) + e^{-TSL/T_{2\rho}}\cdot\sin^2(\beta-\theta)] \tag{14}$$

M returns to –z-axis, with the contamination from $T_{2\rho}$ relaxation.

If δ≠180°, provided $\omega_1 >> \Delta\omega$, θ=90° and $\omega_1 << \Delta\omega$, θ=0°, Equation (13) is simplified as Equation (15) and Equation (16) respectively and artifacts will occur.

$$M_z = M_0(-e^{-TSL/T_{1\rho}} \cdot \sin^2\beta + e^{-TSL/T_{2\rho}} \cdot \cos^2\beta\cos\delta) \quad (15)$$

$$M_z = M_0[e^{-TSL/T_{1\rho}} \cdot \cos^2\beta\cos\delta - e^{-TSL/T_{2\rho}} \cdot \sin^2\beta(\cos^2\partial - \cos\delta\sin^2\partial)] \quad (16)$$

III. Imaging Experiment

The rotary-echo spin-lock pulse (SL pulse B), B_1 and B_0 insensitive composite spin-lock pulse (SL pulse C) and revised B_1 and B_0 insensitive composite spin-lock pulse (SL pulse D) were experimentally tested. Each spin-lock pulse was implemented with Turbo spin-echo (TSE) sequence on a 3T MRI scanner (Philips Medical Systems, Best, The Netherlands). A homogeneous agar phantom was imaged. Body coil was used for excitation so homogeneous B1 field was assumed. A birdcage head coil was used as a receiver. The parameters were set as following: FSL = 50, 250 and 500Hz; TSL = 20ms; TR/TE = 4000/17ms; image matrix size = 144×144; FOV = 20cm^2; slice thickness = 8mm; echo train length = 6; BW = 217Hz/pixel. An interval of 5000ms was inserted after each shot to allow fully recovery of longitudinal magnetization. Fig. 10 presents the B_0 map acquired by the normal dual-TE method (ΔTE=1ms) imaging results. SL pulse C and D are obviously less sensitive to B_0 inhomogeneity.

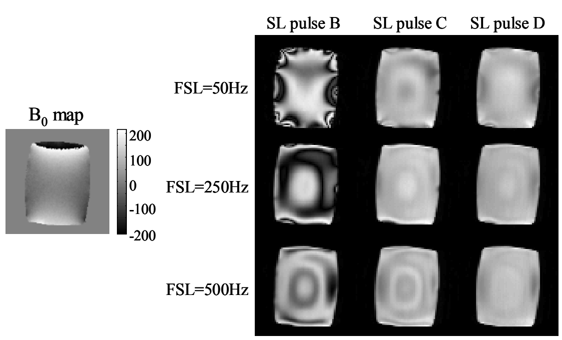

Figure 10. $T_{1\rho}$ weighted images obtained by using SL pulse B, C, D respectively.

IV. Discussion

As identified from the magnetization evolution and imaging results of the investigated spin-lock pulses, imperfect flip angle of tip-down/tip-up/refocus pulse due to inhomogeneous B_1 field will complicate the orientation of the net magnetization. The deviation of the effective spin-lock field from the nominal spin-lock field due to inhomogeneous B_0 further complicates the magnetization evolution and leads to signal null (banding artifact) and/or signal contamination from $T_{2\rho}$ relaxation.

Although composite spin-lock pulses can be used to reduce the spin-lock artifacts associated with B_0 and B_1 field imperfections to different extents, complete elimination of such artifacts is still technically challenging in practice. Improvement of $T_{1\rho}$ quantification can be realized either by reducing artifacts from $T_{1\rho}$-weighted images and then following the simple mono-exponential relaxation model for fitting, or by fitting the signal intensity of $T_{1\rho}$-weighted images even with artifacts to a more complicated magnetization model which is able to quantify $T_{1\rho}$ and $T_{2\rho}$ relaxation even in the presence of field imperfections, as demonstrated in the literature [8]. The former one works at an image acquisition stage; the latter one works at an image post-processing stage. Our study provides a theoretical framework beneficial for both.

This study has some limitations. Phase cycling technique [11] was not analyzed in this study. The theoretical derivation does not account for the transient effect during the spin-lock time. The transient effect may partially explain the incomplete banding compensation by composite spin-lock pulses, in particular for tissues with short T_1 relaxation time. Besides, the phantom imaging demonstration in this study is rather qualitative without taking B_1 inhomogeneities into account. Quantitative evaluation and *in vivo* validation should be further performed in the future studies.

References

[1] Wheaton, A.J. et al, "Proteoglycan loss in human knee cartilage: Quantitation with sodium MR imaging—feasibility study," *Radiology*, vol. 231, pp. 900-905, 2004.

[2] Wang, Y.X. et al, "T1ρ MR imaging is sensitive to evaluate liver fibrosis: An experimental study in a rat biliary duct ligation model," *Radiology*, vol. 259, pp. 712-719, 2011.

[3] Santyr, G.E., Henkelman R.M. and Bronskill M.J., "Spin locking for magnetic resonance imaging with application to human breast," *Magn. Reson. Med.*, vol. 12(1), pp. 25-37, 1989.

[4] Li, X. et al, "Spatial distribution and relationship of T1rho and T2 relaxation times in knee cartilage with osteoarthritis," *Magn. Reson. Med.*, vol. 61(6), pp. 1310-1318, 2009.

[5] Johannessen, W. et al, "Assessment of human disc degeneration and proteoglycan content using T1rho-weighted magnetic resonance imaging," *Spine* (Phila Pa 1976), vol. 31(11), pp. 1253-1257, 2006.

[6] Yuan, J. et al, "Optimized efficient liver $T_{1\rho}$ mapping using limited spin lock times," *Phys. Med. Biol.* vol. 57, pp. 1631–1640, 2012.

[7] Charagundla, S.R. et al, "Artifacts in T1ρ-weighted imaging: Correction with a self-compensating spin-locking pulse," *Journal of Magnetic Resonance*, vol. 162, pp. 113-121, 2003.

[8] Yuan, J. and Wang, Y.-X., "A general T1ρ relaxation model for spin-lock MRI using a rotary echo pulse," *Proc. ISMRM annual meeting*, pp. 124, 2011.

[9] Zeng, H. et al, "A composite spin-lock pulse for ΔB0 + B1 insensitive T1ρ measurement," *Proc. ISMRM annual meeting*, pp. 2356, 2006.

[10] Witschey, II, W.R.T. et al, "Artifacts in T1ρ-weighted imaging: Compensation for B1 and B0 field imperfections," *Journal of Magnetic Resonance*, vol, 186, pp. 75-85, 2007.

[11] W. Chen, et al., "Quantitative T1ρ imaging using phase cycling for B0 and B1 field inhomogeneity compensation," *Magn Reson Imaging*, vol. 29, pp. 608-19, 2011.